The DNLZ/HEP zinc-binding subdomain is critical for regulation of the mitochondrial chaperone HSPA9

Michael T. Vu, Peng Zhai, Juhye Lee, Cecilia Guerra, Shirley Liu, Michael C. Gustin, and Jonathan J. Silberg*

Department of Biochemistry and Cell Biology, Rice University, Houston, Texas 77251

Received 25 August 2011; Revised 4 November 2011; Accepted 27 November 2011
DOI: 10.1002/pro.2012
Published online 7 December 2011 proteinscience.org

Abstract: Human mitochondrial DNLZ/HEP regulates the catalytic activity and solubility of the mitochondrial hsp70 chaperone HSPA9. Here, we investigate the role that the DNLZ zinc-binding and C-terminal subdomains play in regulating HSPA9. We show that truncations lacking portions of the zinc-binding subdomain (ZBS) do not affect the solubility of HSPA9 or its ATPase domain, whereas those containing the ZBS and at least 10 residues following this subdomain enhance chaperone solubility. Binding measurements further show that DNLZ requires its ZBS to form a stable complex with the HSPA9 ATPase domain, and ATP hydrolysis measurements reveal that the ZBS is critical for full stimulation of HSPA9 catalytic activity. We also examined if DNLZ is active *in vivo*. We found that DNLZ partially complements the growth of Δ*zim17 Saccharomyces cerevisiae*, and we discovered that a Zim17 truncation lacking a majority of the C-terminal subdomain strongly complements growth like full-length Zim17. These findings provide direct evidence that human DNLZ is a functional ortholog of Zim17. In addition, they implicate the pair of antiparallel β-strands that coordinate zinc in Zim17/DNLZ-type proteins as critical for binding and regulating hsp70 chaperones.

Keywords: ATPase; chaperone; hsp70; mitochondria; zinc protein

Introduction

Mitochondrial 70 kDa heat shock proteins (mtHsp70) are nuclear-encoded chaperones that are critical for blood development in vertebrates.[1,2] Biochemical and genetic studies have implicated roles for mtHsp70 in numerous mitochondrial processes, including protein folding,[3] translocation,[4] Fe-S cluster biogenesis,[5] and cytochrome c oxidase biogenesis.[6] To fulfill these functions, mtHsp70 binds a diverse array of peptide substrates using its C-terminal peptide-binding domain (PBD). In addition, mtHsp70 uses ATP-binding and hydrolysis by its N-terminal domain to drive conformational changes that regulate peptide-binding affinity.[7,8] Like other hsp70s, mtHsp70 cooperates with multiple auxiliary proteins to complete its cycle of peptide substrate binding and release. DnaJ-type cochaperones target substrates to mtHsp70 by stimulating ATP hydrolysis and promoting formation of a high-peptide affinity conformation,[9] and GrpE-type cochaperones control substrate release by accelerating ADP/ATP exchange and promoting formation of a low-peptide affinity conformation.[10] mtHsp70 is also subject to regulation by the small zinc protein Zim17 (also Hep1/Tim15). Yeast lacking Zim17 accumulate insoluble mtHsp70,[11,12] exhibit mitochondrial defects that mirror those observed upon mtHsp70 depletion,[11,13–15] and display an increase in nuclear-genome recombination.[16]

Additional Supporting Information may be found in the online version of this article.

Grant sponsors: Robert A Welch Foundation C-1614, American Heart Association; Grant sponsor: Friedreich's Ataxia Research Alliance; Grant number: 09BGIA2220299; Grant sponsor: National Science Foundation; Grant number: 1004853.

*Correspondence to: Jonathan J. Silberg, Department of Biochemistry and Cell Biology, Rice University, Houston, TX 77251. E-mail: joff@rice.edu

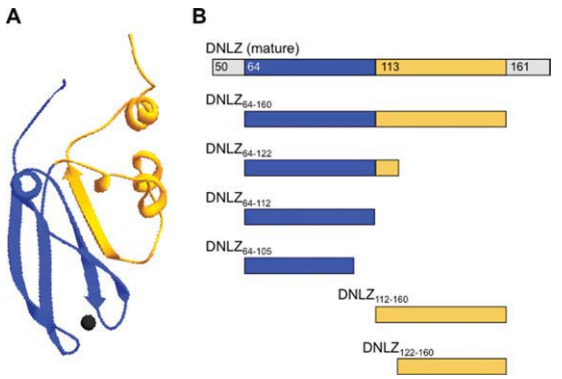

Figure 1. DNLZ truncations mapped onto yeast Zim17. (A) Structure of the trypsin-resistant core of yeast Zim17[24] illustrating the zinc-binding subdomain (*blue*), homologous to DNLZ residues 64–112, and C-terminal subdomain (*yellow*), homologous to DNLZ residues 112–160. Bound Zn^{2+} is shown in black. (B) Diagrams showing the subdomain composition of DNLZ constructs. [Color figure can be viewed in the online issue, which is available at wileyonlinelibrary.com.]

The human DNL-type protein DNLZ (also designated Hsp70 escort protein; HEP) is thought to be a functional ortholog of Zim17. Like Zim17, DNLZ is a nuclear-encoded protein that is translocated to the mitochondria.[17] In addition, DNLZ promotes the solubility of the human mitochondrial chaperone HSPA9, and DNLZ binds strongest to its cognate chaperone in the absence of nucleotides.[17] However, DNLZ and Zim17 display differences in the regulation of their cognate chaperones. DNLZ enhances HSPA9 solubility and stimulates HSPA9 catalytic activity.[17–19] In contrast, Zim17 has only been reported to regulate the solubility of its cognate chaperones.[11–14,20] The finding that DNLZ stimulates the conversion of HSPA9 between its low and high-peptide affinity conformations suggests that DNLZ may regulate the HSPA9 chaperone cycle in addition to HSPA9 solubility. Consistent with the role, a recent study demonstrated that DNLZ prevents the aggregation of a model chaperone substrate,[18] similar to that observed with DnaJ-type cochaperones.[21–23]

Mutagenesis studies have implicated a role for the HSPA9 ATPase domain in mediating binding to DNLZ. A HSPA9 truncation lacking the PBD requires DNLZ for maximal solubility, and the catalytic activity of this truncation is stimulated by DNLZ.[17,19] In addition, DNLZ enhances the solubility of hsp70 chimeras built by fusing the HSPA9 ATPase domain to the PBD of a bacterial chaperone that does not require a Zim17/DNLZ-type protein for solubility.[17] Currently, it remains unclear which DNLZ residues are necessary for binding to and regulating the HSPA9 ATPase domain. A study examining the structure of Zim17 [see Fig. 1(A)] provided evidence that this protein contains a trypsin-resistant core domain that is made up of two compact subdomains.[24] The N-terminal subdomain is made up of a pair of two-stranded β-sheets that coordinate zinc, whereas the C-terminal subdomain contains a mixture of α-helix, β-sheet, and random coil.[24] The zinc-binding subdomain (ZBS) displays the greatest sequence conservation in all Zim17 and DNLZ family members. In addition, this region contains a conserved histidine that is critical for DNLZ regulation of HSPA9,[19] implicating a role for the ZBS in mediating association with mtHsp70 chaperones.

To better understand the role that the ZBS plays in regulating HSPA9, we have investigated the ability of DNLZ truncation mutants to bind HSPA9, regulate chaperone solubility, and stimulate ATP hydrolysis activity. In addition, we have explored whether a DNLZ truncation that regulates recombinant HSPA9 *in vitro* is sufficient to function in yeast.

Results

To investigate which subdomain(s) of DNLZ are required to promote HSPA9 solubility, we constructed six DNLZ truncation mutants [Fig. 1(B)] and examined their effect on chaperone solubility upon expression in *E. coli*. The first mutant, $DNLZ_{64–160}$, contains only those residues that are present in the trypsin-resistant core of Zim17, which complements growth defects of Δ*zim17* yeast.[24] The second mutant, $DNLZ_{64–122}$, includes all the residues from the ZBS as well as 10 residues from the C-terminal subdomain. The third mutant, $DNLZ_{64–112}$, only contains residues from the ZBS. The fourth mutant, $DNLZ_{64–105}$, is truncated within the ZBS, so that it lacks His107, a residue that is critical for stimulating HSPA9 catalytic activity,[17] but includes the tetracysteine motif that is predicted to coordinate zinc.[13,14] The last two mutants, $DNLZ_{112–160}$ and $DNLZ_{122–160}$, lack the ZBS but retain different portions of the C-terminal subdomain.

Figures 2(A) and S2(A) show the effect of each DNLZ truncation on HSPA9 solubility upon expression in *E. coli*. In all experiments, isopropyl-β-D-thiogalactoside (IPTG)-induced expression led to detectable levels of HSPA9. In the presence of $DNLZ_{64–160}$, most of the HSPA9 was observed within the soluble fraction, similar to that observed when HSPA9 was expressed with full-length DNLZ or yeast Zim17.[17] In the presence of $DNLZ_{64–122}$, a majority of the HSPA9 was also present in the soluble fraction, albeit a lower amount than in the presence of $DNLZ_{64–160}$. In contrast, little HSPA9 was detected within the soluble fraction upon coexpression with $DNLZ_{64–112}$, $DNLZ_{64–105}$, $DNLZ_{112–160}$, or $DNLZ_{122–160}$. The steady-state levels of each DNLZ truncation also varied from HSPA9. Each of the variants containing the tetracysteine motif displayed high-steady-state levels upon expression from a T7 promoter like DNLZ,[17] whereas those lacking this motif accumulated to lower levels ($DNLZ_{112–160}$ and $DNLZ_{122–160}$).

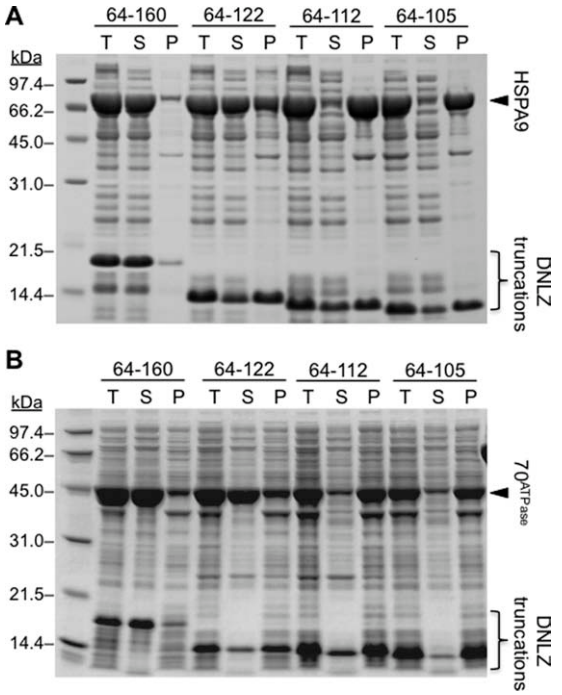

Figure 2. Effect of DNLZ truncations on HSPA9 solubility. SDS–PAGE of *E. coli* expressing different DNLZ truncation and (A) full-length HSPA9 or (B), the HSPA9 ATPase domain. Molecular weight marker [lane 1] and Rosetta 2 *E. coli* harboring a plasmid that expresses HSPA9 and plasmids that express $DNLZ_{64–160}$ [lanes 2–4], $DNLZ_{64–122}$ [lanes 5–7], $DNLZ_{64–112}$ [lanes 8–10], and $DNLZ_{64–105}$ [lanes 11–13]. For each sample, 15 μg of total protein from whole cells (T) is shown as well as the soluble lysate (S) and pellets (P) derived from whole cells that contained the same amount of protein before fractionation.

Furthermore, the solubility of the highly expressed DNLZ truncations differed. A majority of the recombinant $DNLZ_{64–160}$ was observed within the soluble fraction, whereas less than half of $DNLZ_{64–122}$, $DNLZ_{64–112}$, and $DNLZ_{64–105}$ were soluble. The findings that a similar fraction of $DNLZ_{64–122}$ and $DNLZ_{64–112}$ was within the soluble cellular fraction upon coexpression with HSPA9 provide evidence that differences in their abilities to promote HSPA9 solubility cannot be attributed to variation in their solubility. The low-expression level of $DNLZ_{112–160}$ and $DNLZ_{122–160}$ made it difficult to quantify their solubility (Supporting Information Fig. S2), although the finding that these proteins could be purified from cell lysates indicates that they are at least partially soluble upon expression in *E. coli*.

Figures 2(B) and S2(B) show the effect of each DNLZ variant on the solubility of an HSPA9 truncation that contains only the ATPase domain and interdomain linker, 70^{ATPase}. IPTG-induced expression of 70^{ATPase} in the presence of $DNLZ_{64–160}$ or $DNLZ_{64–122}$ yielded a majority of the chaperone in the soluble fraction, similar to that observed with full-length DNLZ.[17] In contrast, the other DNLZ variants did not affect the solubility of 70^{ATPase}. Taken together with our solubility analysis of full-length HSPA9, these results demonstrate that a 59-residue DNLZ fragment, including the entire ZBS and 10 residues extending into the C-terminal subdomain, is sufficient to maintain HSPA9 as a soluble protein. They also show that this activity arises from an interaction with HSPA9 through its ATPase domain and/or interdomain linker.

The differing abilities of DNLZ truncations to promote HSPA9 solubility could arise because they bind zinc and acquire structure to differing extents. To test this, five truncations were purified using a strategy similar to that reported for DNLZ,[17,19] and the stoichiometry of bound zinc was measured by mixing each truncation with an excess of methyl methanethiolsulphonate (MMTS) and monitoring the level of zinc released using 4-(2-pyridylazo) resorcinol (PAR), a zinc chelator that exhibits increased absorbance at 500 nm upon zinc binding.[25] Like full-length DNLZ,[17] the level of zinc released upon addition of MMTS was near stoichiometric for all truncations containing the tetracysteine motif (Table I). In contrast, only trace amounts of Zn^{2+} were found in $DNLZ_{112–160}$, the truncation lacking the tetracysteine motif.

We also used spectropolarimetry to analyze the secondary structure of two active ($DNLZ_{64–160}$ and $DNLZ_{64–122}$) and two inactive ($DNLZ_{64–112}$ and $DNLZ_{112–160}$) truncations. Figure 3 shows the mean residue ellipticity between 190 and 260 nm for each variant. The spectrum for $DNLZ_{112–160}$ lacks intense minima near wavelengths where α-helix (208 and 222 nm) and β-sheet (215 nm) secondary structure produce the largest negative ellipticity, but instead exhibits a single minimum at a wavelength (199 nm) where random coil proteins produce large negative ellipticity. In contrast, the spectra for $DNLZ_{64–160}$, $DNLZ_{64–122}$, and $DNLZ_{64–112}$ contain two minima (near 205 and 219 nm), consistent with the presence of mixed α-helix and β-sheet content as observed in the spectrum of the Zim17 trypsin-resistant core domain.[24] These results provide evidence that the ZBS retains structure in the absence of the C-terminal subdomain, whereas the C-terminal subdomain does not display structure in isolation.

To determine whether the defects in $DNLZ_{64–112}$ and $DNLZ_{112–160}$ arise because they do not form stable complexes with the HSPA9 ATPase domain,[17] the binding of these truncations to 70^{ATPase} was analyzed using gel filtration and compared to that of $DNLZ_{64–160}$ and $DNLZ_{64–122}$. Figure 4 shows the

Table I. *Zinc Content in Purified Truncations*

Protein	Zn^{2+} stoichiometry
$DNLZ_{64–160}$	1.198 ± 0.034
$DNLZ_{64–122}$	0.863 ± 0.005
$DNLZ_{64–112}$	1.024 ± 0.001
$DNLZ_{64–105}$	0.871 ± 0.009
$DNLZ_{112–160}$	0.091 ± 0.002

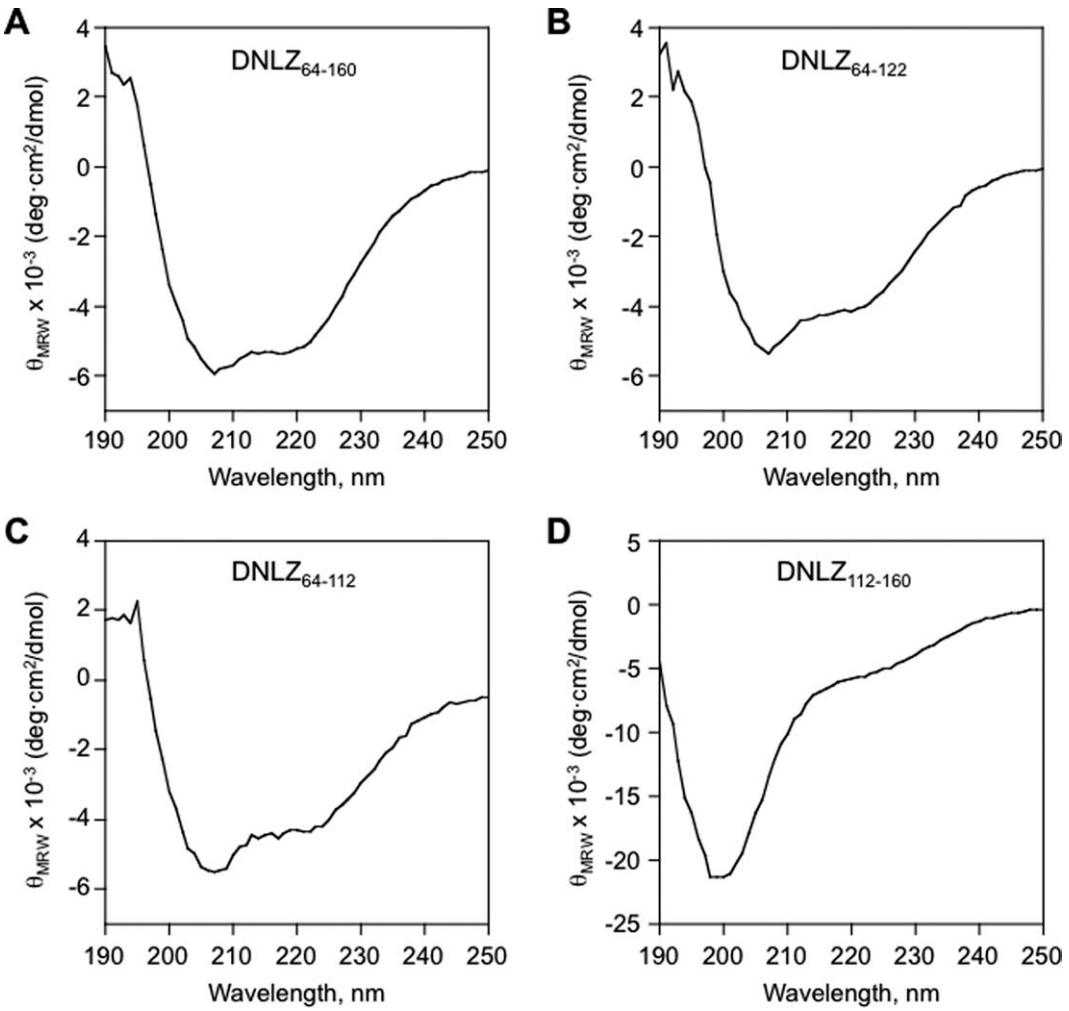

Figure 3. Far UV circular dichroism spectra of (A) $DNLZ_{64–160}$, (B) $DNLZ_{64–122}$, (C) $DNLZ_{64–112}$, and (D) $DNLZ_{112–160}$ at 25°C. The protein concentrations used were 10 μ*M*, and elipticity data are presented on a mean residue basis. Buffer: 10 m*M* phosphate pH 7.4 and 1 m*M* DTT.

elution profiles for 70^{ATPase}, each DNLZ truncation, and mixtures of 70^{ATPase} with each DNLZ variant. The individual DNLZ truncations eluted as monodisperse peaks with elution volumes consistent with that expected for monomeric proteins. $DNLZ_{64–160}$ eluted at a MW_{app} = 23.1 kDa (MW_{calc} = 15.4 kDa), $DNLZ_{64–122}$ eluted at a MW_{app} = 15.9 kDa (MW_{calc} = 11.5 kDa), $DNLZ_{64–112}$ eluted at a MW_{app} = 15.9 kDa (MW_{calc} = 10.4 kDa), and $DNLZ_{112–160}$ eluted at a MW_{app} = 12.6 kDa (MW_{calc} = 10.4 kDa). 70^{ATPase} also eluted as a monodisperse peak with an apparent molecular mass (MW_{app} = 36.2 kDa) similar to that calculated for a monomer (MW_{calc} = 43.8 kDa) as previously observed.[17] The lower than expected MW_{app} suggests that this protein associates with the matrix of the column. Figure 4 also shows that two of the DNLZ truncations alter the elution of 70^{ATPase}. In the presence of $DNLZ_{64–160}$ and $DNLZ_{64–122}$, 70^{ATPase} displayed MW_{app} (58.7 and 49.7 kDa, respectively) that are higher than that observed with 70^{ATPase} alone (36.2 kDa). In contrast, $DNLZ_{64–112}$ and $DNLZ_{112–160}$ did not alter the elution of 70^{ATPase} when present at equimolar levels or when present at a concentration that is five-fold higher than 70^{ATPase} (data not shown).

The finding that $DNLZ_{64–122}$ enhances the solubility of HSPA9 in *E. coli* and binds to its ATPase domain implicates a 59-residue fragment containing the full ZBS as sufficient for regulating HSPA9. To test if this fragment stimulates HSPA9 ATP hydrolysis like full-length DNLZ,[17,18] we used a coupled-enzyme assay to measure the rate of phosphate production by HSPA9 in the presence of a concentration of each truncation (40 μ*M*) that is 10-fold higher than the HSPA9 K_M for DNLZ.[17] Figure 5(A) shows that $DNLZ_{64–160}$ and $DNLZ_{64–122}$ enhanced the HSPA9 rate of ATP hydrolysis to a similar extent as DNLZ (14–17-fold). $DNLZ_{64–112}$ and $DNLZ_{112–160}$ also stimulated HSPA9 activity; however, the level of stimulation (five to sevenfold) was lower. Figure 5(B) shows the effect of each DNLZ variant on 70^{ATPase} activity. With this HSPA9 construct, only $DNLZ_{64–160}$ stimulated chaperone ATPase activity to a similar extent as DNLZ. $DNLZ_{64–122}$ and $DNLZ_{112–160}$

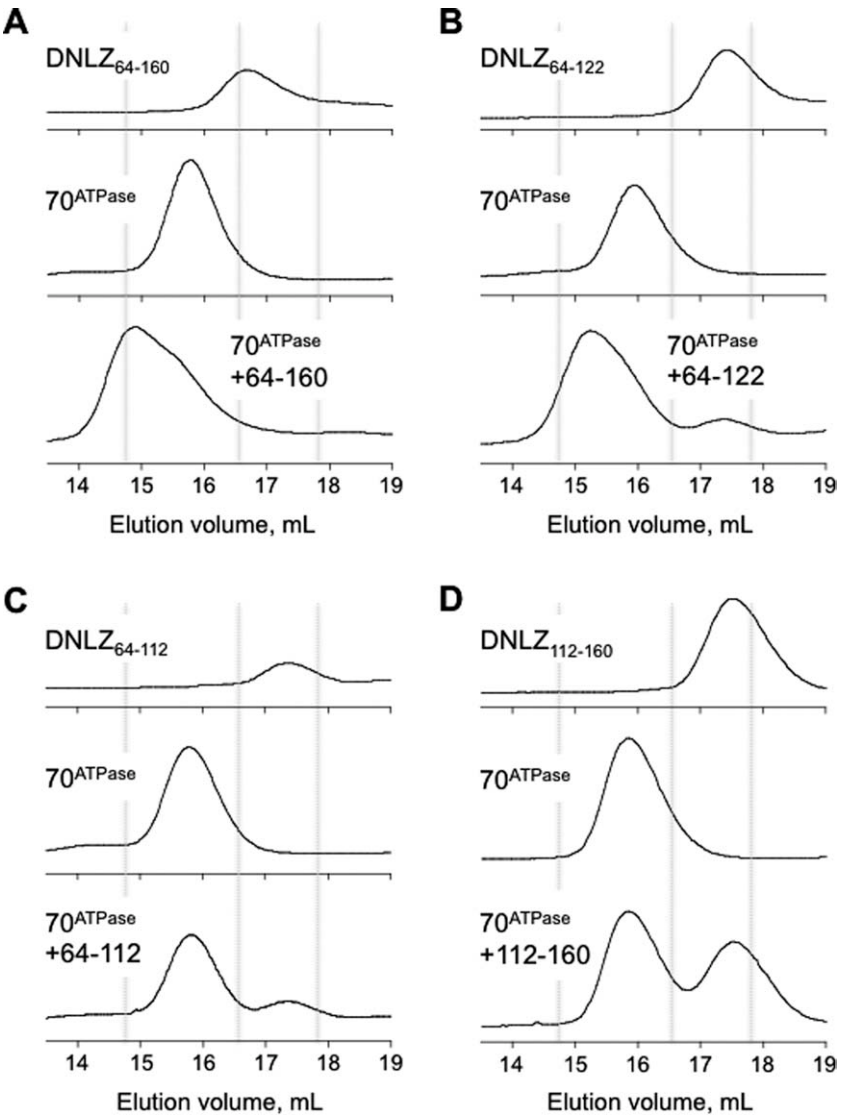

Figure 4. Gel filtration analysis of HSPA9 and DNLZ truncation binding. Effect of mixing the HSPA9 ATPase domain and (A) $DNLZ_{64–160}$, (B) $DNLZ_{64–122}$, (C) $DNLZ_{64–112}$, and (D) $DNLZ_{112–160}$ on elution from a Superdex 200 10/300 GL column chromatographed using HKMD buffer at 4°C. The volume of sample injected (100 μL) and protein concentrations (20 μ*M*) were identical in all experiments. The dashed lines indicate the volumes where the standards bovine serum albumin (66 kDa), carbonic anhydrase (29 kDa), and cytochrome C (12.4 kDa) eluted.

both had negligible effects on 70^{ATPase} activity, whereas $DNLZ_{64–112}$ decreased 70^{ATPase} activity. Analysis of chaperone solubility revealed that this occurs in part because $DNLZ_{64–112}$ and 70^{ATPase} aggregate in the presence of ATP (data not shown).

DNLZ is predicted to be a functional ortholog of yeast Zim17, because these proteins display 25% sequence identity and enhance the solubility of mitochondrial hsp70 chaperones.[17–19] Further support for this comes from the finding that Zim17 promotes the solubility of HSPA9 upon overexpression in *E. coli*.[17] To test if human DNLZ is a functional ortholog of Zim17, the gene encoding human DNLZ was cloned into a yeast shuttle vector, and the ability of this plasmid to rescue the growth defect of Δ*zim17 S. cerevisiae* was compared to a vector expressing yeast Zim17. Figure 6 shows that yeast cells lacking Zim17 were not viable on synthetic complete dextrose (SCD) medium-containing 5-FOA at 30°C, whereas cells expressing Zim17 from a plasmid were viable under these conditions, similar to that previously reported.[14,24] In addition, cells harboring a plasmid expressing human DNLZ grew in the presence of 5-FOA. However, this DNLZ complementation strength was less than that observed with cells expressing yeast Zim17. To test whether the 59-residue fragment of DNLZ that binds 70^{ATPase} *in vitro* is also functional in mitochondria, a stop codon was incorporated into the DNLZ expression vector, so that translation is terminated after residue 122. Unlike full-length DNLZ, this vector did not support the growth of Δ*zim17* yeast in the presence of 5-

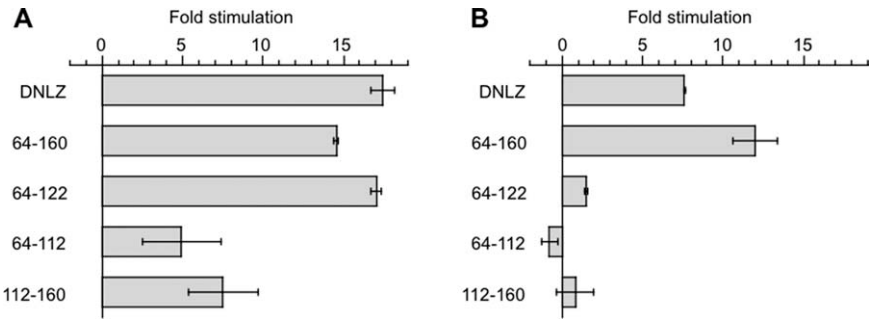

Figure 5. Stimulation of HSPA9 ATP hydrolysis by DNLZ truncations. The ATPase activities of (A) full-length HSPA9 [5 μ*M*] and (B) the HSPA9 ATPase domain [5 μ*M*] were measured under steady-state conditions [1 m*M* ATP] in the presence and absence of full-length DNLZ and DNLZ truncations [40 μ*M*]. First-order rates were measured in TKMD buffer at 25°C and are reported as the fold stimulation over the intrinsic activities of HSPA9 and the ATPase domain, respectively. The data shown represent the average of three independent experiments with error bars corresponding to ±1 standard deviation.

FOA. However, a vector expressing a homologous truncation of Zim17 (residues 1–121) complemented Δ*zim17* growth under similar conditions. Similar complementation results were observed with each construct when experiments were performed at 37°C.

Discussion

Two subdomains were previously observed in the structure of a functional trypsin-resistant fragment of Zim17.[24] The N-terminal subdomain of this fragment consists of a pair of antiparallel β-sheets, which are thought to directly coordinate zinc, whereas the C-terminal subdomain contains a mixture of α-helix, β-sheet, and random coil, which make intermolecular contacts with the ZBS.[24] *In vivo* studies with Zim17 mutants further implicated the tetracysteine motif in the N-terminal subdomain as critical for the *in vivo* function of Zim17. Point mutations at cysteines in this motif disrupt protein function,[14] presumably because Zim17 requires these residues to coordinate zinc and acquire structure.[24] In addition, mutations of charged residues within the Zim17 zinc-binding and C-terminal subdomains were found to abrogate Zim17 function within yeast.[24] Among these mutations, the most severe defects were observed with substitutions within the N-terminal ZBS. Similarly, *in vitro* studies examining the effects of mutations on human DNLZ activity found that the strongest functional defects occur with a mutation in the ZBS,[19] implicating this region as critical for binding to hsp70 chaperones.

The results described herein provide direct evidence that the ZBS is critical for forming a DNLZ-HSPA9 complex, whereas much of the C-terminal subdomain is dispensable. $DNLZ_{64–160}$ and $DNLZ_{64–122}$, truncations containing the full ZBS, both increase the solubility of full-length HSPA9 and its isolated ATPase domain upon expression in *E. coli*. In addition, these truncations form a stable complex with the HSPA9 ATPase domain in the absence of nucleotide that can be detected using gel filtration chromatography. This can be contrasted with truncations containing residues from the ZBS alone ($DNLZ_{64–112}$) and the C-terminal subdomain ($DNLZ_{112–160}$). These truncations do not enhance chaperone solubility, and they do not form a stable complex with the HSPA9 ATPase domain in the absence of nucleotide. With $DNLZ_{64–112}$, the inability to enhance HSPA9 solubility does not appear to be due to changes in its solubility or structure. The expression and solubility of this variant in *E. coli* mirror that of the functional $DNLZ_{64–122}$, as does its zinc content and secondary structure content. This suggests that the 10 residues following the DNLZ subdomain boundary are either directly involved in mediating binding to HSPA9 or required to maintain the ZBS in a conformation that is competent for complex formation.

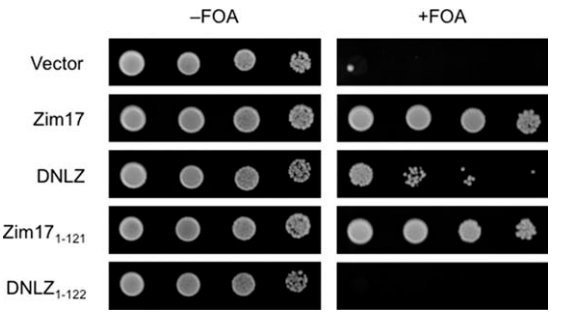

Figure 6. Complementation of yeast Δ*zim17*. Relative growth at 30°C of a Δ*zim17/pURAScZim17* yeast haploid strain transformed with the p415GPD lacking an insert (vector) and p415GPD-derived vectors that expresses yeast Zim17 (Zim17), human DNLZ (DNLZ), residues 1–121 of Zim17 ($Zim17_{1–121}$), and residues 1–122 of DNLZ ($DNLZ_{1–122}$). The spots represent a dilution series of cells (1×, 10×, 100×, and 1,000×) spotted onto SCD plates lacking (−FOA, 48 h) or containing 5-FOA (+FOA, 96 h), which were obtained from SCD liquid cultures (−uracil/−leucine) containing 300 μg/mL G418. Representative spots are shown from selections performed in triplicate.

Studies examining truncation effects on HSPA9 ATP hydrolysis implicate a role for the DNLZ ZBS in regulating HSPA9 activity. DNLZ truncations containing all the residues from the ZBS and portions of the CTD, $DNLZ_{64–160}$ and $DNLZ_{64–122}$, stimulate the steady-state activity of full-length HSPA9 to a similar extent as DNLZ when they are present at a concentration that is 10-fold higher than the HSPA9 K_M for DNLZ.[17] Truncations composed of the isolated subdomains ($DNLZ_{64–112}$ and $DNLZ_{112–160}$) also stimulate HSPA9 activity. However, the level of stimulation with these truncations is lower than that observed with larger fragments of DNLZ. This smaller stimulation could arise because maximal HSPA9 rate enhancement requires an interaction between DNLZ and both HSPA9 domains, that is, the ATPase and PBDs. Surprisingly, $DNLZ_{64–122}$ does not stimulate the isolated HSPA9 ATPase domain strongly like full-length chaperone. This weaker stimulation suggests that $DNLZ_{64–122}$ lacks residues from the C-terminal subdomain (residues 123–160) that are critical for strong stimulation of the HSPA9 ATPase domain. Future studies will be required to determine if residues from the C-terminal subdomain contact both HSPA9 domains, or if they are required to maintain DNLZ in a conformation that is competent for effectively stimulating ATPase domain activity.

Our yeast complementation experiments provide the first demonstration that human DNLZ is a functional ortholog of yeast Zim17. As previously observed, a vector that constitutively expresses yeast Zim17 complements the growth of Δ*zim17 S. cerevisiae*.[14,24] Similarly, a vector designed to constitutively express human DNLZ complements the growth of Δ*zim17* yeast, albeit to a lesser extent than yeast Zim17. Complementation studies with this strain further revealed that a Zim17 truncation lacking the majority of the C-terminal subdomain supports Δ*zim17* growth like Zim17. This provides evidence that the ZBS and 10 residues following the subdomain boundary are sufficient for binding and regulating hsp70 chaperones within living cells, similar to that observed with DNLZ and HSPA9 *in vitro*. However, a homologous DNLZ truncation does not complement this strain. This could arise because the DNLZ truncation accumulates to lower steady-state levels or because this DNLZ truncation exhibits a decreased affinity for the yeast chaperones Ssc1 and Ssq1, which become insoluble in the absence of Zim17.[15]

Although the studies herein provide evidence for a direct interaction between fragments of DNLZ and HSPA9, the cellular role(s) for its chaperone regulation remains unclear. Furthermore, the finding that the DNLZ C-terminal subdomain is dispensable for HSPA9 binding raises the question about the function(s) of this region. Sequence comparisons of mitochondrial and plastid homologs of DNLZ reveal that C-terminal subdomains are present in other family members.[13,26] However, the sequence conservation in this subdomain is lower than that observed in the ZBS, and the C-terminal subdomain varies almost twofold in length, unlike the ZBS, which has a conserved length.[26] Our studies herein indicate that the C-terminal subdomain is required for DNLZ solubility. Truncations expressed in *E. coli* display decreased solubility when this subdomain is removed, and these proteins aggregate upon freeze thawing after purification. In addition, our results suggest that the DNLZ C-terminal subdomain interacts with the HSPA9 PBD. Support for this comes from the finding that the isolated C-terminal subdomain of DNLZ stimulates the catalytic activity of full-length HSPA9 but does not form a stable complex with the HSPA9 ATPase domain or affect its activity. Unfortunately, we were unable to test whether the C-terminal subdomain is also required for the chaperone activity of DNLZ. In isolation, both DNLZ subdomains display decreased solubility in the presence of the model chaperone substrate denatured rhodanese (data not shown), whose aggregation is suppressed by full-length DNLZ.[18]

Future studies will be required to differentiate the possible functions for the DNLZ C-terminal subdomain. This subdomain may be important for regulating the activity and solubility of the ZBS, inhibiting formation of HSPA9-substrate complexes, and/or targeting chaperone substrates to hsp70s like J-type cochaperones.[27] Additional studies are also needed to establish the exact residues in DNLZ and HSPA9 that directly mediate their association as well as the cellular role(s) for DNLZ-type regulation. DNLZ could be important for blood development in vertebrates like HSPA9.[1,2] Furthermore, DNLZ may be needed to maintain HSPA9 solubility in the cytosol of human cancer cells, where the level of this hsp70 is enriched[28,29] and where HSPA9 regulates centrosome duplication.[30]

Materials and Methods

Materials

E. coli XL1-Blue and Rosetta 2 cells were from Stratagene and EMD Biosciences, respectively, and the *S. cerevisiae* Δ*zim17*/*ZIM17* strain was from OpenBiosystem. Enzymes for DNA manipulation were obtained from Roche Biochemical, New England Biolabs, and Promega. Synthetic oligonucleotides were obtained from Fischer Scientific, pET vectors were from EMD Biosciences, and pRS415GPD and pRS416 vectors were from ATCC. NuPAGE Novex 10% Bis–Tris gels from Invitrogen were used for all electrophoresis experiments. Bacterial and yeast growth media components were from BD Biosciences, and gentamicin sulfate (G418) and 5′-

fluoroorotic acid (5-FOA) were from Fisher Scientific. All other reagents were from Sigma-Aldrich.

Vectors

The vectors used for expressing DNLZ (pHis-Hep), HSPA9 ATPase domain (pATPase-His), and full-length HSPA9 (pHsp70-His) without mitochondrial targeting sequences were described previously.[17] A gene fragment encoding the residues in DNLZ (64–160) that is homologous to the trypsin-resistant core of *S. cerevisiae* Zim17[24] was PCR amplified from pHis-Hep and cloned into pET30a vector at NcoI and HindIII sites (pDNLZ::64–160). The codons for DNLZ residues 123, 113, and 106 were mutated to stop codons in pDNLZ::64–160 using Quikchange mutagenesis to create pDNLZ::64–122 (residues 64–122), pDNLZ::64–112 (residues 64–112), and pDNLZ::64–105 (residues 64–105). The pDNLZ::64–160 plasmid was amplified using primers that introduce NotI sites before the codons encoding residues 112 or 122, and the amplicons from these reactions were digested with NotI and circularized by ligation to obtain pDNLZ::112–160 and pDNLZ::122–160. The gene-encoding HSPA9 residues 47–440 was PCR amplified from pATPase-His and cloned into pET19b using NdeI and BamHI to create pET19b-70ATPase, a vector that expresses this protein with an N-terminal enterokinase removable His tag.

To create a vector that supports growth of a haploid Δ*zim17* strain in the absence but not in the presence of 5-FOA, the *ZIM17* gene and its promoter were PCR amplified from yeast genomic DNA (chromosome 14 and regions 52661–51687) and cloned into the centromeric plasmid pRS416[31] using XbaI and HindIII to create pURA-ScHep1. Vectors for complementation analysis were generated by PCR amplifying the genes encoding full-length human DNLZ and yeast Zim17 from pHep-EGFP[17] and a *S. cerevisiae* genomic DNA (BY4743, OpenBiosystem) and cloning the amplicons into the centromeric yeast plasmid pRS415GPD[31] using XbaI and HindIII restriction sites. The resulting vectors use a GPD promoter to constitutively express DNLZ (p415HsHEP) and Zim17 (p415ScHep1). Quikchange mutagenesis was used to introduce stop codons into p415HsDNLZ and p415ScZim17 to create vectors that express variants of DNLZ and Zim17 (p415HsHEP::1–122 and p415ScHep1::1–121) that are truncated at structurally related sites. All constructs were sequence verified.

Protein purification

Recombinant DNLZ and HSPA9 were expressed and purified as previously described.[17] Each DNLZ truncation was also purified using a procedure similar to that reported for DNLZ.[17] Rosetta 2 (DE3) cells transformed with pET vectors that express each mutant were grown at 37°C, induced to express protein with 0.1 m*M* IPTG at an $A_{600} \cong 0.4$–0.7, and grown for ≈19 h at 23°C to allow for expression. Harvested cells were resuspended in TND buffer [50 m*M* Tris, pH 8.0, 150 m*M* NaCl, and 1 m*M* dithiothreitol (DTT)] containing 1 m*M* $MgCl_2$, 300 μg/mL lysozyme, 2 U/mL DNase I and Complete, EDTA-free Protease Inhibitor Cocktail. After two −80°C freeze/thaw cycles, lysed cells were centrifuged at 40,000*g* to remove cell debris. Cleared lysate was applied to Ni-NTA agarose column equilibrated in TND buffer, the column was washed with TND buffer containing 15 m*M* imidazole to remove unbound protein, and His-tagged truncations were eluted with TND buffer containing 150 m*M* imidazole. Eluted protein was dialyzed against 10 m*M* Tris pH 8.5 and 1 m*M* DTT buffer. The protein was concentrated and chromatographed using an S-75 Superdex column (GE Healthcare) in 10 m*M* Tris pH 8.5, 1 m*M* DTT buffer, and fractions appearing homogeneous were pooled and concentrated to ≥200 μ*M*. The yields for DNLZ truncations containing a full ZBS were 4–40 mg/L culture, whereas the yields for DNLZ truncations lacking portions of this subdomain were 0.8–1.7 mg/L culture. This can be contrasted with the yield for full-length DNLZ, which is ≥80 mg/L culture. Unlike full-length DNLZ, the DNLZ truncations aggregated to differing extents after a single freeze-thaw, and so all biochemical measurements were performed on freshly purified proteins that had not been frozen. SDS–PAGE of purified DNLZ truncations is provided in Supporting Information Figure S1.

The ATPase domain (70^{ATPase}) expressed from pET19b-70ATPase was purified as described for constructs containing a C-terminal His tag.[17] However, purified 70^{ATPase} protein (∼10 mg/mL) was treated with 1 U/mL enterokinase (EMD Bioscience) for 72 h at 23°C and applied to HisTrap column to remove the affinity tag and uncleaved protein. 70^{ATPase} was further chromatographed using an S-75 column (GE Healthcare), and fractions appearing homogeneous were pooled and concentrated to ≥200 μ*M*.

Escort activity screen

Rosetta 2 *E. coli* transformed with pHsp70[17] or pET19b-70ATPase in the absence and presence of vectors that express DNLZ truncations were grown at 37°C in LB to mid-logarithmic phase, induced to express proteins by adding 0.1 m*M* IPTG, and grown for ∼18 h at 23°C. Cells were harvested by centrifugation, resuspended in TND buffer (50 m*M* Tris pH 8.0, 150 m*M* NaCl, and 1 m*M* DTT) containing 1 m*M* $MgCl_2$, 300 μg/mL lysozyme, 2 U/mL DNase I, and frozen at −80°C overnight. Lysed cells were thawed, the total protein concentration was determined using the Bio-Rad Protein Assay, and the lysate was centrifuged at 40,000*g* to separate the insoluble and soluble proteins. The insoluble fractions

were resuspended in TND buffer to the same volume as the soluble fraction before analysis using SDS–PAGE.

ATPase assays

Steady-state ATP hydrolysis rates were measured using the EnzCheck phosphate detection kit (Invitrogen) as previously described.[27,32] Hydrolysis activity of HSPA9 and 70^{ATPase} was analyzed in TKMD (50 m*M* Tris pH 8.0, 150 m*M* KCl, 10 m*M* $MgCl_2$, and 1 m*M* DTT) buffer. Reactions were performed by incubating all components except ATP for 5 min at 25°C and then initiating reactions by adding ATP to a final concentration of 1 m*M*. The effects of DNLZ variants on HSPA9 catalytic activity are reported as fold stimulation of the intrinsic rates observed in the absence of DNLZ. Error bars represent ± one standard deviation.

Zinc stoichiometry

Purified DNLZ truncations were incubated in 50 m*M* HEPES pH 7.5 containing 100 μ*M* PAR—a zinc chelator[25]—and 200 μ*M* MMTS, a reagent that displaces zinc by reacting with sulfhydryl ligands.[33] After a 60-min incubation, the concentration of the PAR-$(Zn^{2+})_2$ complex was determined by measuring the absorbance at 500 nm. The amount of zinc released was calculated using an extinction coefficient for PAR-$(Zn^{2+})_2$ (ε_{500} = 59,052 M^{-1} cm^{-1}) that was generated using a $ZnCl_2$ standard curve. Measurements were performed in triplicate using 6.6 μ*M* protein, corrected for the level of zinc in the buffer, and are reported as the average value ±1 standard deviation.

Gel filtration chromatography

DNLZ truncation and 70^{ATPase} binding were examined using an analytical Superdex 200 10/300 GL column, driven by an AKTA fast-protein liquid chromatography system (GE Healthcare). Elution profiles are shown for proteins analyzed at 4°C using HKMD running buffer (50 m*M* HEPES, pH 7.4, 150 m*M* KCl, 10 m*M* $MgCl_2$, and 1 m*M* DTT) lacking nucleotide. For experiments analyzing complex formation, identical concentrations of 70^{ATPase} and DNLZ (20 μM each) were incubated together in running buffer for 30 min at 4°C before injection over the column. A standard curve for estimating molecular weights was generated using: amylase (200 kDa), bovine serum albumin (66 kDa), carbonic anhydrase (29 kDa), cytochrome C (12.4 kDa), and aprotinin (6.4 kDa). Experiments performed in TKMD buffer (pH 8) yielded similar elution profiles.

Yeast complementation

The *S. cerevisiae* heterozygote YSC1021-669052,[34] which has one of its chromosomal *zim17* (also *hep1/tim15)* genes replaced by *kanMX* (*MAT*a/α *his3Δ1/his3Δ1 leu2Δ/leu2Δ LYS2/lys2Δ met15Δ/MET15 ura3Δ/ura3Δ HEP1::KanMX/HEP1*), was transformed with pURA-ScHep1 using the EZ Transformation II kit (Zymo research), and a haploid strain (Δ*zim17*/pURA3-ScHep1) was obtained by sporulation followed by tetrad dissection using the random spore isolation method.[35] The isolated spores were grown on agar plates containing SCD medium (–uracil) and 300 μg/mL G418. To screen for *met15*Δ haploids, colonies were patched onto agar plates containing complete or minus methionine SCD and 300 μg/mL G418.

The haploid Δ*zim17*/pURA-ScHep1 strain was transformed with centromeric vectors (pRS415GPD derived) that express each variant (DNLZ, $DNLZ_{1–122}$, Zim17, and $Zim17_{1–121}$) using the Frozen-EZ Yeast transformation II kit (Zymo Research). Transformed cells were grown on agar plates containing –leucine drop-out medium and 300 μg/mL G418. Colonies harboring plasmids that express DNLZ and Zim17 were identified by PCR screening with primers that amplify their genes. Protein complementation of Δ*zim17*/pURA-ScHep1 was analyzed by growing colonies in SCD liquid medium (–uracil/–leucine) containing 300 μg/mL G418 to an optical density ~2 in SCD medium, plating 10 μL dilutions of this culture (corresponding to an OD of 1, 0.1, 0.01, and 0.001) on agar plates containing SCD medium ±1 mg/mL 5-FOA, and imaging growth after 48 (0 mg/mL 5-FOA) and 96 h (1 mg/mL 5-FOA). The previously described haploid Δ*zim17* strain[12,15] available from Euroscarf (#10179B) was not used, because its growth could not be complemented by p415ScHep1.

Analytical methods

Absorbance and ellipticity measurements were performed using a Cary 50 UV–vis spectrophotometer and JASCO 815 spectropolarimeter, respectively.

References

1. Chen TH, Kambal A, Krysiak K, Walshauser MA, Raju G, Tibbitts JF, Walter MJ (2011) Knockdown of Hspa9, a del(5q31.2) gene, results in a decrease in hematopoietic progenitors in mice. Blood 117:1530–1539.
2. Craven SE, French D, Ye W, de Sauvage F, Rosenthal A (2005) Loss of Hspa9b in zebrafish recapitulates the ineffective hematopoiesis of the myelodysplastic syndrome. Blood 105:3528–3534.
3. Kang PJ, Ostermann J, Shilling J, Neupert W, Craig EA, Pfanner N (1990) Requirement for hsp70 in the mitochondrial matrix for translocation and folding of precursor proteins. Nature 348:137–143.
4. Schneider HC, Berthold J, Bauer MF, Dietmeier K, Guiard B, Brunner M, Neupert W (1994) Mitochondrial Hsp70/MIM44 complex facilitates protein import. Nature 371:768–774.
5. Voisine C, Schilke B, Ohlson M, Beinert H, Marszalek J, Craig EA (2000) Role of the mitochondrial Hsp70s, Ssc1 and Ssq1, in the maturation of Yfh1. Mol Cell Biol 20:3677–3684.

6. Fontanesi F, Clemente P, Barrientos A (2011) Cox25 teams up with Mss51, Ssc1, and Cox14 to regulate mitochondrial cytochrome c oxidase subunit 1 expression and assembly in *Saccharomyces cerevisiae*. J Biol Chem 286:555–566.
7. Palleros DR, Reid KL, Shi L, Welch WJ, Fink AL (1993) ATP-induced protein-Hsp70 complex dissociation requires K+ but not ATP hydrolysis. Nature 365: 664–666.
8. Schmid D, Baici A, Gehring H, Christen P (1994) Kinetics of molecular chaperone action. Science 263: 971–973.
9. Qiu XB, Shao YM, Miao S, Wang L (2006) The diversity of the DnaJ/Hsp40 family, the crucial partners for Hsp70 chaperones. Cell Mol Life Sci 63:2560–2570.
10. Schmidt S, Strub A, Rottgers K, Zufall N, Voos W (2001) The two mitochondrial heat shock proteins 70, Ssc1 and Ssq1, compete for the cochaperone Mge1. J Mol Biol 31313–31326.
11. Sanjuan Szklarz LK, Guiard B, Rissler M, Wiedemann N, Kozjak V, van der Laan M, Lohaus C, Marcus K, Meyer HE, Chacinska A, Pfanner N, Meisinger C. (2005) Inactivation of the mitochondrial heat shock protein zim17 leads to aggregation of matrix hsp70s followed by pleiotropic effects on morphology and protein biogenesis. J Mol Biol 351:206–218.
12. Blamowska M, Sichting M, Mapa K, Mokranjac D, Neupert W, Hell K (2010) ATPase domain and interdomain linker play a key role in aggregation of mitochondrial Hsp70 chaperone Ssc1. J Biol Chem 285: 4423–4431.
13. Burri L, Vascotto K, Fredersdorf S, Tiedt R, Hall MN, Lithgow T (2004) Zim17, a novel zinc finger protein essential for protein import into mitochondria. J Biol Chem 279:50243–50249.
14. Yamamoto H, Momose T, Yatsukawa Y, Ohshima C, Ishikawa D, Sato T, Tamura Y, Ohwa Y, Endo T (2005) Identification of a novel member of yeast mitochondrial Hsp70-associated motor and chaperone proteins that facilitates protein translocation across the inner membrane. FEBS Lett 579:507–511.
15. Sichting M, Mokranjac D, Azem A, Neupert W, Hell K (2005) Maintenance of structure and function of mitochondrial Hsp70 chaperones requires the chaperone Hep1. EMBO J 24:1046–1056.
16. Diaz de la Loza MD, Gallardo M, Garcia-Rubio ML, Izquierdo A, Herrero E, Aguilera A, Wellinger RE (2011) Zim17/Tim15 links mitochondrial iron-sulfur cluster biosynthesis to nuclear genome stability. Nucleic Acids Res 39:6002–6015.
17. Zhai P, Stanworth C, Liu S, Silberg JJ (2008) The human escort protein Hep binds to the ATPase domain of mitochondrial hsp70 and regulates ATP hydrolysis. J Biol Chem 283:26098–26106.
18. Goswami AV, Chittoor B, D'Silva P (2010) Understanding the functional interplay between mammalian mitochondrial Hsp70 chaperone machine components. J Biol Chem 285:19472–19482.
19. Zhai P, Vu MT, Hoff KG, Silberg JJ (2011) A conserved histidine in human DNLZ/HEP is required for stimulation of HSPA9 ATPase activity. Biochem Biophys Res Commun 408:589–594.
20. Pareek G, Samaddar M, D'Silva P (2011) Primary sequence that determines the functional overlap between mitochondrial heat shock protein 70 Ssc1 and Ssc3 of *Saccharomyces cerevisiae*. J Biol Chem 286: 19001–19013.
21. Cyr DM (1995) Cooperation of the molecular chaperone Ydj1 with specific Hsp70 homologs to suppress protein aggregation. FEBS Lett 359:129–132.
22. Szabo A, Korszun R, Hartl FU, Flanagan J (1996) A zinc finger-like domain of the molecular chaperone DnaJ is involved in binding to denatured protein substrates. EMBO J 15:408–417.
23. Deloche O, Liberek K, Zylicz M, Georgopoulos C (1997) Purification and biochemical properties of *Saccharomyces cerevisiae* Mdj1p, the mitochondrial DnaJ homologue. J Biol Chem 272:28539–28544.
24. Momose T, Ohshima C, Maeda M, Endo T (2007) Structural basis of functional cooperation of Tim15/Zim17 with yeast mitochondrial Hsp70. EMBO Rep 8: 664–670.
25. Hunt JB, Neece SH, Ginsburg A (1985) The use of 4-(2-pyridylazo)resorcinol in studies of zinc release from *Escherichia coli* aspartate transcarbamoylase. Anal Biochem 146:150–157.
26. Willmund F, Hinnenberger M, Nick S, Schulz-Raffelt M, Muhlhaus T, Schroda M (2008) Assistance for a chaperone: chlamydomonas HEP2 activates plastidic HSP70B for cochaperone binding. J Biol Chem 283: 16363–16373.
27. Silberg JJ, Tapley TL, Hoff KG, Vickery LE (2004) Regulation of the HscA ATPase reaction cycle by the cochaperone HscB and the iron-sulfur cluster assembly protein IscU. J Biol Chem 279:53924–53931.
28. Wadhwa R, Takano S, Kaur K, Deocaris CC, Pereira-Smith OM, Reddel RR, Kaul SC (2006) Upregulation of mortalin/mthsp70/Grp75 contributes to human carcinogenesis. Int J Cancer 118:2973–2980.
29. Yi X, Luk JM, Lee NP, Peng J, Leng X, Guan XY, Lau GK, Beretta L, Fan ST (2008) Association of mortalin (HSPA9) with liver cancer metastasis and prediction for early tumor recurrence. Mol Cell Proteom 7: 315–325.
30. Ma Z, Izumi H, Kanai M, Kabuyama Y, Ahn NG, Fukasawa K (2006) Mortalin controls centrosome duplication via modulating centrosomal localization of p53. Oncogene 25:5377–5390.
31. Mumberg D, Muller R, Funk M (1995) Yeast vectors for the controlled expression of heterologous proteins in different genetic backgrounds. Gene 156:119–122.
32. Silberg JJ, Vickery LE (2000) Kinetic characterization of the ATPase cycle of the molecular chaperone Hsc66 from *Escherichia coli*. J Biol Chem 275:7779–7786.
33. Smith DJ, Maggio ET, Kenyon GL (1975) Simple alkanethiol groups for temporary blocking of sulfhydryl groups of enzymes. Biochemistry 14:766–771.
34. Winzeler EA, Shoemaker DD, Astromoff A, Liang H, Anderson K, Andre B, Bangham R, Benito R, Boeke JD, Bussey H, Chu AM, Connelly C, Davis K, Dietrich F, Dow SW, El Bakkoury M, Foury F, Friend SH, Gentalen E, Giaever G, Hegemann JH, Jones T, Laub M, Liao H, Liebundguth N, Lockhart DJ, Lucau-Danila A, Lussier M, M'Rabet N, Menard P, Mittmann M, Pai C, Rebischung C, Revuelta JL, Riles L, Roberts CJ, Ross-MacDonald P, Scherens B, Snyder M, Sookhai-Mahadeo S, Storms RK, Véronneau S, Voet M, Volckaert G, Ward TR, Wysocki R, Yen GS, Yu K, Zimmermann K, Philippsen P, Johnston M, Davis RW. (1999) Functional characterization of the *S. cerevisiae* genome by gene deletion and parallel analysis. Science 285:901–906.
35. Rockmill B, Lambie EJ, Roeder GS (1991) Spore enrichment. Methods Enzymol 194:146–149.